Journal of Biomechanics 104 (2020) 109705

Contents lists available at ScienceDirect

Journal of Biomechanics

journal homepage: www.elsevier.com/locate/jbiomech
www.JBiomech.com

Short communication

Correction of bias in the estimation of cell volume fraction from histology sections

Yanxin Liu [a], Andrea G. Schwartz [b], Yuan Hong [a,d,e], Xiangjun Peng [a,d,e], Feng Xu [e], Stavros Thomopoulos [c], Guy M. Genin [a,d,e,*]

[a] Department of Mechanical Engineering & Materials Science, Washington University in St. Louis, United States
[b] Department of Orthopaedic Surgery, Washington University School of Medicine, United States
[c] Department of Orthopedic Surgery, Department of Biomedical Engineering, Columbia University, United States
[d] NSF Science and Technology Center for Engineering Mechanobiology, Washington University in St. Louis, United States
[e] Bioinspired Engineering and Biomechanics Center, School of Life Sciences and Technology, Xi'an Jiaotong University, China

ARTICLE INFO

Article history:
Accepted 20 February 2020

Keywords:
Homogenization theory
Histology
Quantitative stereology

ABSTRACT

Accurate determination of the fraction of a tissue's volume occupied by cells is critical for studying tissue development, pathology, and biomechanics. For example, homogenization methods that predict the function and responses of tissues based upon the properties of the tissue's constituents require estimates of cell volume fractions. A common way to estimate cellular volume fraction is to image cells in thin, planar histologic sections, and then invoke either the Delesse or the Glagolev principle to estimate the volume fraction from the measured area fraction. The Delesse principle relies upon the observation that for randomly aligned, identical features, the expected value of the observed area fraction of a phase equals the volume fraction of that phase, and the Glagolev principle relies on a similar observation for random rather than planar sampling. These methods are rigorous for analysis of a polished, opaque rock sections and for histologic sections that are thin compared to the characteristic length scale of the cells. However, when histologic slices cannot be cut sufficiently thin, a bias will be introduced. Although this bias – known as the Holmes effect in petrography – has been resolved for opaque spheres in a transparent matrix, it has not been addressed for histologic sections presenting the opposite problem, namely transparent cells in an opaque matrix. In this note, we present a scheme for correcting the bias in volume fraction estimates for transparent components in a relatively opaque matrix.

1. Introduction

The volume fractions of cells and extracellular matrix (ECM) in a tissue are important parameters in quantitative biology and biomechanics. For example, when considering electrical conduction or the mechanics of tissues, the volume fractions of constituents are key metrics for relating the behavior of tissues to the behaviors of their constituents (Milton, 2002; Saadat et al., 2015; Soares and Sacks, 2016; Genin and Birman, 2009; Marquez et al., 2005a,b; Wagenseil et al., 2003). The physical properties of cells and ECM themselves also vary with volume fraction (Marquez et al., 2006, 2010; Genin and Elson, 2014), and with the local electro-mechanical environment (Nekouzadeh et al., 2008; Lee et al., 2012; Thomopoulos et al., 2011; Genin et al., 2011). In bimaterial attachments (Thomopoulos et al., 2012) such as those at the attachment of tendon to bone, gradients (Thomopoulos et al., 2006; Genin et al., 2009) are believed to be important to tissue function, including gradients in cell volume fraction that vary over time (Thomopoulos et al., 2010). These distributions of cell volume fraction are determinants of the local stress environment around cells, a factor so important that it appears to be conserved across species at the attachment of tendon to bone (Liu et al., 2014; Deymier-Black et al., 2015; Saadat et al., 2016).

For all of these reasons, accurate estimation of cellular volume fraction is critical. A challenge is that these estimates must often be made using histologic sections (e.g., Fig. 1). Additionally, spatial gradients of cell populations and staining are common in histology (Fig. 2), making it challenging to simply search for perfectly sectioned, archetypal cells. In the best of cases, volume fraction estimation can be achieved using either the Delesse or the Glagolev principle (Delesse, 1847; Haug, 1986; Mouton, 2002) over relevant portions of an image, and estimates of volume fraction can be

* Corresponding author.
E-mail address: genin@wustl.edu (G.M. Genin).

https://doi.org/10.1016/j.jbiomech.2020.109705
0021-9290/

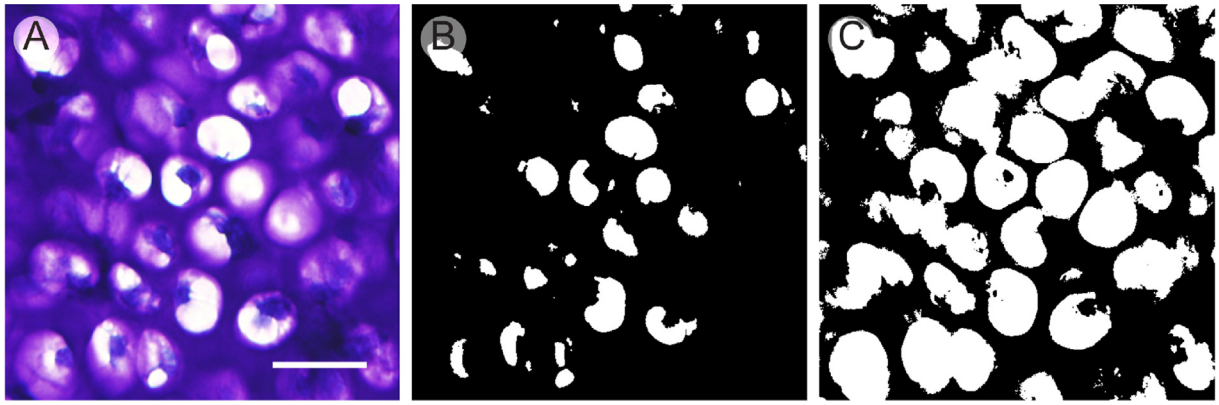

Fig. 1. (a) A 12 μm thick toluidine blue-stained tissue section containing murine chondrocytes. The image is shown with a minimum (b) or maximum (c) cell area threshold (white areas) illustrating the potential under- or over-estimate of cell area fraction that could arise from interpreting this image. Scale bar: 50 μm.

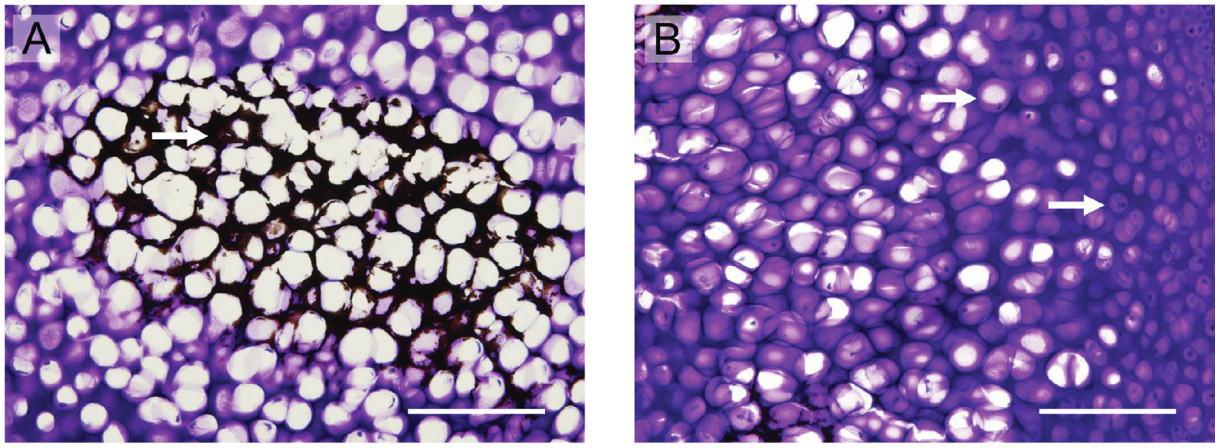

Fig. 2. In many histology sections analogous to that in Fig. 1, gradients in (a) stain and (b) cell size exist, meaning that volume fraction estimation must proceed over subsections of an image. In such cases, bias error estimation is especially important because the chances of finding a few archetypal cells with perfect slicing in each area is lower. As in Fig. 1, a 12 μm thick Toluidine blue-stained tissue section containing murine chondrocytes is shown. Scale bars: 100 μm.

made through sufficient sampling to avoid unbiased error (Mouton, 2014). The Delesse principle relates the area of an object found on a planar section to its volume fraction. The Glagolev principle takes advantage of faster convergence to exact volume fractions when random sampling is made over such planar sections. The conditions for these to yield accurate estimates of volume fraction are that the components be distributed homogeneously throughout a tissue and that the plane of transection be representative of the whole tissue. However, this is seldom the case in biologic systems. If one could examine all possible planes of transection and compute the true mean intercepted areas for each component within the containing volume, then the volume fraction of the component would equal the quotient of the mean intercepted areas of the component and the containing volume (Mayhew and Cruz, 1973; Mayhew and Cruz Orive, 1974):

$$\frac{V_C}{V_T} = \frac{E(A_C)}{E(A_T)} \tag{1}$$

where $E(.)$ represents the expected exact value, the subscript C represents the component of interest within the volume, the subscript T represents the entire space sampled including that occupied by the component of interest, and A denotes area and V denotes volume.

In practice, estimates must be made from a finite number of planes of transection, and one must test against unbiased error in estimates of $E(A_C)$ and $E(A_T)$ through rigorous and randomized sampling procedures. If these conditions are met, the volume fraction can be estimated from the mean area of the component and containing volume (Mayhew and Cruz Orive, 1974):

$$\frac{V_C}{V_T} \sim \frac{\overline{A}_C}{\overline{A}_T} \tag{2}$$

As the sampling size increases, the estimate accuracy improves. If the area of the containing volume A_T is constant, the volume fraction of any component contained within its volume can be estimated from the mean of the area fraction, $\overline{A}_C$:

$$\frac{V_C}{V_T} = E\left(\frac{A_C}{A_T}\right) \sim \left(\frac{\overline{A}_C}{A_T}\right) \tag{3}$$

For cases of non-constant intercepted area A_T, Eqs. (1)–(3) are approximations.

In addition to these sources of unbiased error, there exist sources of biased error for analysis of images of partially transparent sections of finite thickness. This is especially true when the section thickness is comparable to the representative dimension of the measured components. The Holmes effect in petrography is one example of how bias arises from the failure to observe true areas of inclusions within a volume due to the finite thickness of slices (Weibel et al., 1966; Mouton, 2002): the apparent area A_C of an opaque component contained within a slice of an otherwise transparent volume will always be that of the component's maxi-

mum cross-section within the slice rather than the true area at the predetermined plane of transection. Thus, the sampling of the opaque component area A_C will be biased, leading to overestimation of volume fraction. Chayes (Chayes, 1956) derived a correction for the Holmes effect for the case of opaque spherical particles of constant radius R:

$$\frac{E(A_t)}{E(A_a)} = \frac{4R}{4R+3t} \tag{4}$$

where the lower case subscript t represents true area and the subscript a represents the apparent area. t is the thickness of thin section.

In histology, depending on the staining method chosen, the converse scenario may occur. For example, in the case of a toluidine blue stained chondrocyte-containing tissue (Fig. 1), transparent cells are contained within an opaque matrix. The apparent area of cellular component observed will be that of its minimum cross section in the thin section, and the relative area and hence volume fraction of the component will generally be underestimated.

Although the correction for the Holmes effect is well established, there has not been a treatment of this converse scenario of which we are aware. We therefore developed a quantitative estimate of degree of volume fraction underestimation when the transparent components of interest are spherical or ellipsoidal in shape. We tested it against data for which the matrix was not completely opaque and for which bounds on volume fraction could be estimated by image thresholding.

2. Theory

2.1. Spherical components

Consider an idealized tissue with spherical cells of radius R situated in a cubic lattice of spacing a so that each sphere resides at the center of a cubic unit cell of edge length a (Fig. 3). The true mean intercepted area for the spherical component is:

$$E(A_C) = \frac{\pi}{a}\int_{-R}^{R}\left(R^2-\Delta^2\right)d\Delta = \frac{\frac{4}{3}\pi R^3}{a} \tag{5}$$

Then,

$$\frac{E(A_C)}{E(A_T)} = \frac{\frac{4}{3}\pi R^3}{a^3} \tag{6}$$

is the true volume fraction of the spherical component, as the Delesse principle states. Δ represents the z coordinate of each plane of transection.

Now consider the case where the thickness for each plane of transection is t, and assume the top layer is the true observed area to be measured (Fig. 3b). There are three critical positions at which the measured area fraction of component at the top of the slice is larger than or equal to the bottom of slice. These critical sets of sectioning planes are displayed as dashed lines in Fig. 4. For each example, the area of the cell measured at the bottom of the slice is smaller than that measured at the top of the slice. If the matrix is opaque, the projected area measured will be the minimum area within the slice, introducing bias into the measurement of A_C. To quantify this, we investigate the case $a/2 > R+t$, so that the top layer of the planes of transection will intercept all the possible planes within the sphere.

If $t < 2R$, the measured area for every plane of transection will be underestimated by:

$$\begin{aligned} E(A_C)^* \cdot a \quad &= \int_{-R-t}^{-R}\pi\left[R^2-(\Delta+t)^2\right]d\Delta + \int_{-R}^{-t/2}\pi\left[\left(R^2-(\Delta+t)^2\right)\right. \\ &\left.-\left(R^2-\Delta^2\right)\right]d\Delta = \pi\left(tR^2-\tfrac{t^3}{12}\right) \end{aligned} \tag{7}$$

where the superscript $*$ denotes the area difference between the smaller bottom layer and larger top layer and Δ represents the z coordinate of the lower plane of the section of thickness t.

Thus, the fraction by which the mean intercepted area is underestimated is a function of t and R. The under-estimation of the true volume fraction of the cells can thus be written:

$$k = \left(\frac{V_C}{V_T}\right)^* / \left(\frac{V_C}{V_T}\right) = \frac{E(A_C)^*}{E(A_C)} \tag{8}$$

so that the fraction of under-estimation of the true volume fraction is:

$$k = \frac{\left(tR^2-\frac{t^3}{12}\right)}{\frac{4}{3}R^3} = \frac{3t}{4R} - \frac{1}{16}\left(\frac{t}{R}\right)^3 \tag{9}$$

If $t > 2R$, the observed area of the component in an opaque containing volume will be zero.

2.2. Aligned ellipsoidal components

The morphology of many cells is more ellipsoidal than spherical. Here, we derive the underestimation of volume fraction for cells that are ellipsoidal with the following form:

$$\frac{x^2}{b^2}+\frac{y^2}{b^2}+\frac{z^2}{c^2} = 1,$$

with $b < c$, and with the long axis of the cell aligned perpendicular to the imaging plane.

The procedure follows that used for spherical components, and provides a similar result. The true mean intercepted area for an ellipsoidal component is:

$$E(A_C) = \frac{\pi b^2\int_{-c}^{c}\left(1-\frac{\Delta^2}{c^2}\right)d\Delta}{a} = \frac{\frac{4}{3}\pi b^2 c}{a} \tag{10}$$

Similarly, considering the case $\frac{a}{2} > c+t$, with slice thickness $t < 2c$

$$\begin{aligned} E(A_C)^* \cdot a \quad &= \int_{-c-t}^{-c}\pi b^2\left[1-\tfrac{(\Delta+t)^2}{c^2}\right]d\Delta \\ &+ \int_{-c}^{-t/2}\pi b^2\left[\left(1-\tfrac{(\Delta+t)^2}{c^2}\right)-\left(1-\tfrac{\Delta^2}{c^2}\right)\right]d\Delta \\ &= \tfrac{\pi b^2}{c^2}\left(tc^2-\tfrac{t^3}{12}\right) \end{aligned} \tag{11}$$

The fraction by which the true volume fraction is expected to be underestimated is thus:

$$k = \frac{3t}{4c} - \frac{1}{16}\left(\frac{t}{c}\right)^3 \tag{12}$$

As with spherical components, the degree of under-estimation depends on the thickness to cell size ratio t/c. If $t > 2c$, no cells are visible through the opaque matrix.

3. Computational methods

To assess the convergence towards our predictions, we generated simulated microscopy slices containing a volume fraction of $\phi = 0.05$ of ellipsoidal cells with an aspect ratio (short axes:long axis) of $b:c = 0.31$ or spherical cells with $b:c = 1$ using a custom code in Matlab (The Mathworks, Natick, MA). This code generated images with a prescribed number of pixels of finite thickness sections through the simulated tissue. Matrix was taken as opaque, and cells as fully transparent, so that all pixels were set to 0 if the sum of the distances between the pixel center and the two elliptical foci was greater than twice the length of the long axis

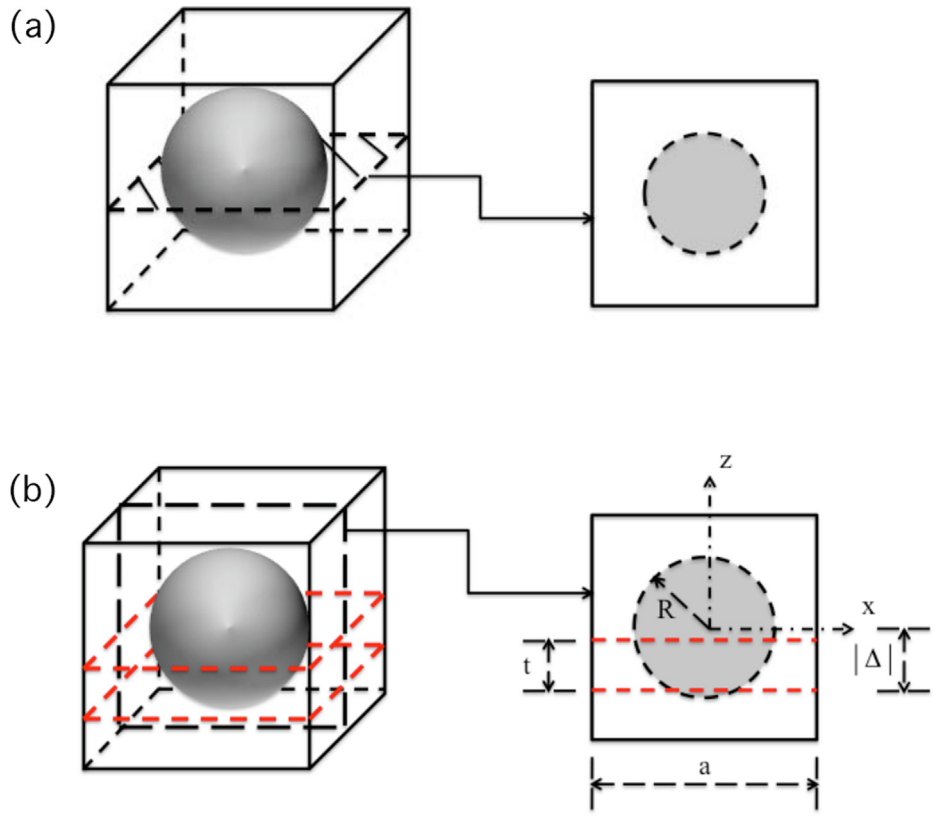

Fig. 3. (a) The volume fraction of ellipsoids, including spheres, within a matrix can be estimated from polished sections or infinitesimally thin slices using via either the Glagolev or Delesse principle. The mean area fraction, A_T/a^2, is equivalent to the volume fraction of the spherical constituent. (b) A transection plane of finite thickness t through this same composite, representative of a histology slice. Regions between two dashed planes (red online) represent the slices of transection plane. The 2D figure on the right is the view of the vertical xz plane through the center. As evident in Fig. 1, a range of estimates of A_T/a^2 are possible from such a slice.

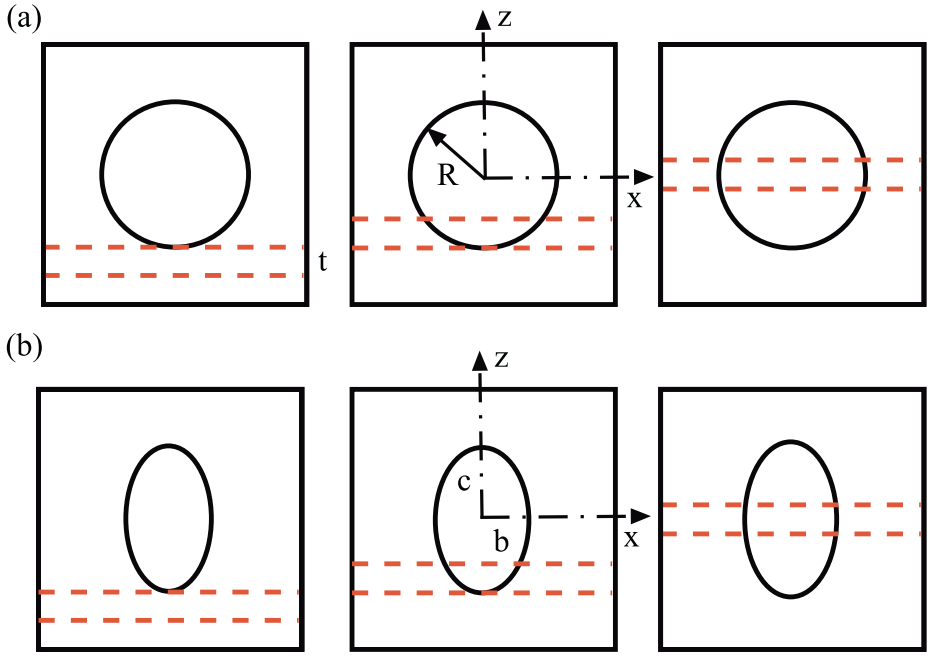

Fig. 4. For three critical slices, the cross-sectional area of the inclusion on the top of the slice is no smaller than that on bottom. This is the case for both (a) a spherical inclusion and (b) and ellipsoidal inclusion.

of the cell, 2c, and to 1 otherwise. The positions of the centers of cells in the direction perpendicular to the imaging plane were chosen randomly from a uniform distribution. Cells were spaced uniformly on a square lattice to ensure no overlap. Effective volume fractions were calculated by determining the area fraction of non-occluded space for slices of prescribed thickness.

To establish the limits of the approach for cells that are oriented randomly, additional simulations were performed in which orientations of the long axes of the cells were chosen from a uniform spherical distribution. Spacing of cells along the imaging axis was random; because no overlap was allowed, some cells had to be repositioned to maintain $\phi = 0.05$.

4. Results and discussion

Estimating the volume fraction from a measured area fraction is a commonly encountered problem when analyzing the mechanical behavior of biological tissues. In doing so, it is important to ensure that the containing area is constant throughout all the planes of transection, as by Mayhew and Cruz Orive (Mayhew and Cruz Orive, 1974). When the thickness of a histology section is not negligible relative to the size of the cells, the measured area will be inaccurate resulting in a biased estimate of the volume fraction of the components. Chayes (Chayes, 1956) derived a correction for the case of opaque spherical components of constant radius in a transparent containing volume. In this case, the observed area will be the maximum possible area of inclusions in the slice.

In this note, we give a quantitative description of the opposite scenario: the case of an opaque containing volume with spherical or ellipsoidal transparent inclusions. This method is effective when cross-sections contain a sufficient number of cells that the effects of cases outside the scope of our error estimation correction are rare (Fig. 4), such as when the thickness of the transection plane is larger than the diameter of the components aligned with the transection plane thickness direction and there is thus no observed area of the cells.

When the thickness of the transection plane is not large compared to cell components, the under-estimation of the expected value of the cell area is related to the ratio of the section thickness to the size of the inclusions (Fig. 5). For aligned ellipsoidal cells, error is small for relatively thin histologic sections, and rises to 100% for sections that are thick compared to the cells. To place this into the context of commonly applied imaging schemes in which estimation of volume fractions could be desired, we make reference to confocal fluorescence microscopy and histological slices of cartilage and fibrocartilage, two orthopedic tissues containing chondrocyte cells whose shape is actively maintained to be ellipsoidal (Grashoff et al., 2003). In the context of confocal fluorescence microscopy, volume fractions of cells can be estimated by staining the ECM and optically sectioning the tissue (Wong et al., 1996). This optical sectioning enables a region of approximately

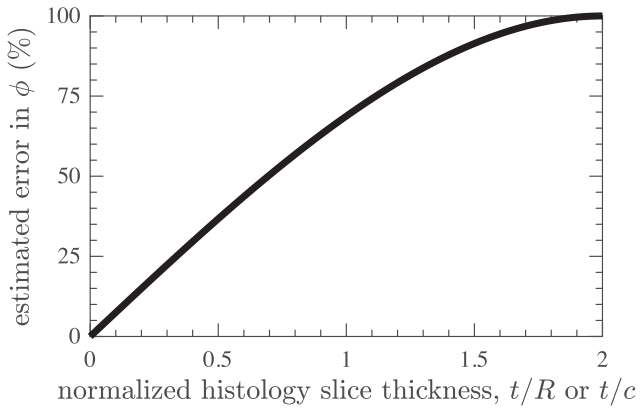

Fig. 5. The estimation bias in volume fraction, ϕ, for thick slices can be predicted for both spherical inclusions of radius R and ellipsoidal inclusions of major axis c aligned perpendicular to the transection plane for cases when the matrix is opaque compared to the inclusion. Here, t is the thickness of the transection plane.

$t = 500$ nm thickness to be selected from a cell that is on the order of $2R = 12$ micrometers in diameter, depending upon osmotic conditions (Guilak et al., 2002). For such a case, the error associated with occlusion of the cell diameter can be found to be small from Fig. 5: for t/R = 0.083, the expected underestimation in volume fraction is on the order of 5%. This can of course be compensated for in confocal fluorescence microscopy by reconstructing entire cells and interpolating the true diameter (Guilak et al., 2002). Additionally, improvements in ultramicrotome sectioning of tissues at low temperatures enable the production of specimens that are thin compared to most eukaryotic cells (Plumley et al., 2019).

For the case of a histology slice like that in Fig. 1, the problem is more pronounced. In this case, the thickness of the histology slice is on the order of 5–10 micrometers thick, meaning t/R on the order of $0.5 - 1$ and underestimation of volume fraction on the order of 35–65%. Here, no analogous workaround exists, and the Delesse and Glagolev principles are the logical approach to estimating volume fractions from these slices.

The Delesse and Glagolev approaches both rely upon having sufficient numbers of cell images to obtain a meaningful estimate. Additionally, estimates improve with increasing image resolution. To assess the rate of convergence towards our estimates, we performed two computational studies. In the first, we considered aligned cells with a volume fraction of 0.05 and assessed the estimates as a function of slice thickness and number of pixels in an area of matrix containing a single cell. 100 cells were imaged for each slice thickness considered. For fewer than 16 by 16 pixels per area corresponding to a single cell, too few cells were visible in our images to estimate a volume fraction. For the three slice thicknesses considered, the estimates converged to our model for more than 32 by 32 pixels per cell area (Fig. 6). The thickest slice considered had an estimated volume fraction approximately 10–20% below the model's predictions, likely due to numerous cells that did not penetrate both ends of the slice. Convergence towards the model was independent of the aspect ratio of the cell.

In the second assessment, we considered how the volume fraction estimate converged to the model as a function of the number of cells imaged for the case of cells imaged at 32 by 32 pixels over an area corresponding to a single cell (Fig. 7). The volume fraction estimates followed our model with increasingly fidelity as the number of cells imaged increased. For thinner sections, as few as 10 images were sufficient for very good convergence.

Although many cells such as cardiomyocytes, fibroblasts, and chondrocytes tend to align in three dimensional tissues and culture, especially when stressed (Grashoff et al., 2003; Spencer et al., 2016; De et al., 2007; Zemel and Safran, 2007), they often transition from a disordered to an ordered state during maturation of tissue constructs in a way that is strongly influenced by the boundary conditions (Wang et al., 2014; Abhilash et al., 2014; Svoronos et al., 2013). In these earlier stages, cells typically adopt a more rounded morphology (Elson and Genin, 2016), so that the orientation distribution is less critical. To assess the error associated with having a random distribution of cells, we repeated the simulations, but this time with orientations of the long axis of the ellipse oriented in a direction that was chosen randomly from a spherical orientation distribution (Fig. 8). An additional problem arises in these cells, in that having an orientation skewed from the perpendicular to the imaging plane can lead to further occlusion of the cell area, especially for cells oriented close to 45° to the imaging plane. This leads to a larger under-prediction of volume fraction than predicted by our model.

Many cells are not well approximated by ellipsoids. Because of the problem of cell processes that are thin compared to the slice thickness being occluded by the ECM, these processes can be entirely missed when using the Delesse or Glagolev principle to estimate the volume fractions of cells in an opaque matrix. The

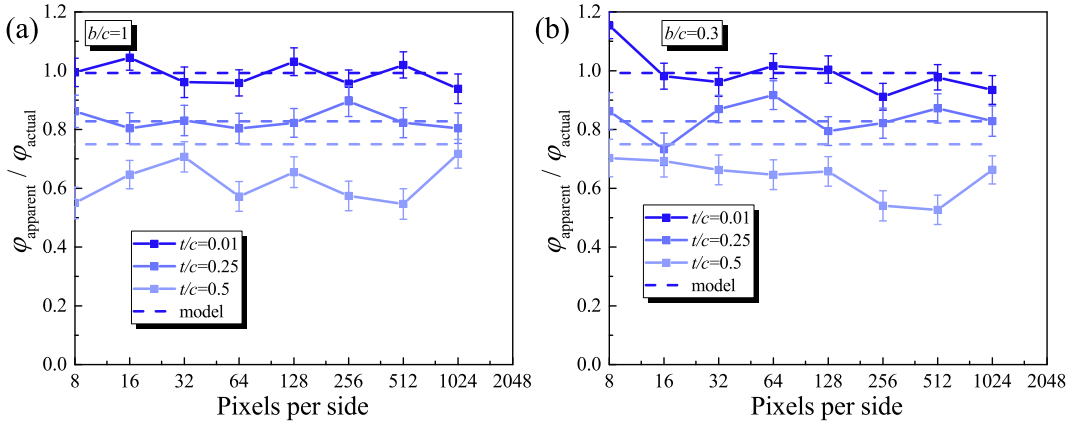

Fig. 6. Simulations of the underestimation of volume fraction for cells in a relatively thick opaque matrix, with data shown mean ± standard error. 100 simulated cells were imaged for each image size, with the image size corresponding to the number of pixels on the side of a cubic region that contains a single cell. The long axes of cells were aligned with the normal to the imaging plane. (a) Spherical cells, and (b) ellipsoidal cells with aspect ratio $b/c = 0.3$.

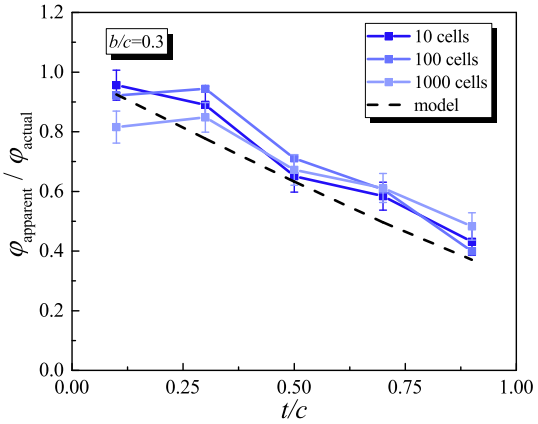

Fig. 7. Simulations of the underestimation of volume fraction for cells in a relatively thick opaque matrix, with data shown mean ± standard error. The deviation from the model increased with increasing slice thickness t/c, and decreased with the number of cells imaged. Each cell occupied an area of matrix that was 256 by 256 pixels. Ellipsoidal cells were chosen with $b/c = 0.3$, and with the long axes of cells aligned perpendicular to the imaging plane.

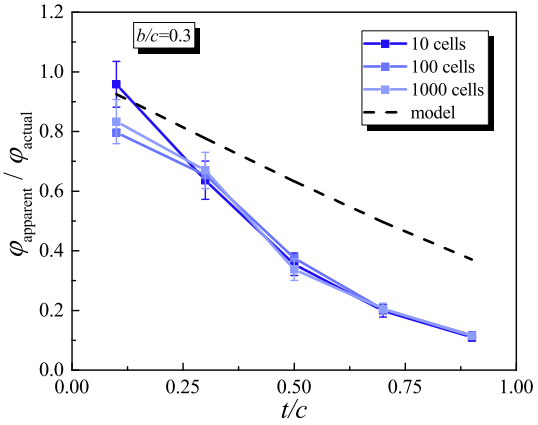

Fig. 8. Simulations of the underestimation of volume fraction for randomly oriented cells in a relatively thick opaque matrix, with data shown mean ± standard error. The deviation from the model increased with increasing slice thickness t/c, and decreased with the number of cells imaged. Each cell occupied an area of matrix that was 256 by 256 pixels. Ellipsoidal cells were chosen with $b/c = 0.3$, and with the long axes of cells aligned in a direction that was chosen from a uniform spherical distribution.

errors in measurement in these conditions are not accounted for by our model. This would pose a significant issue for cells such as axons, which extend cell processes that can be long compared to their cell bodies and that can sustain a significant proportion of their volume (Lee et al., 1986). The problem is lesser for fibroblasts, which extend cell processes during remodeling of their ECM that typically engulf a much smaller fraction of the cell volume (Heath and Peachey, 1989).

Ideally, one should try to limit the section thickness to avoid inaccuracy in the volume fraction estimate when using Delesse principle. However, when this is not possible, the procedure described within this note can be used to limit bias in the measurement for cases of reasonably ellipsoidal, aligned cells with processes that do not hold a significant proportion of the cell's volume.

Declaration of Competing Interest

The authors declare that they have no known competing financial interests or personal relationships that could have appeared to influence the work reported in this paper.

Acknowledgments

This work was funded in part by the National Institutes of Health through grant U01EB016422, and by the National Science Foundation through the NSF Science and Technology Center for Engineering Mechanobiology, grant CMMI 1548571.

References

Abhilash, A., Baker, B.M., Trappmann, B., Chen, C.S., Shenoy, V.B., 2014. Remodeling of fibrous extracellular matrices by contractile cells: predictions from discrete fiber network simulations. Biophys. J . 107, 1829–1840.
Chayes, F., 1956. Petrographic Modal Analysis: An Elementary Statistical Appraisal. Wiley.
De, R., Zemel, A., Safran, S.A., 2007. Dynamics of cell orientation. Nat. Phys. 3, 655.
Delesse, A., 1847. Precede mechanique pour determines la composition de roches (extrait). C.R. Acad. Sci. (Paris) 25, 544–560.
Deymier-Black, A.C., Pasteris, J.D., Genin, G.M., Thomopoulos, S., 2015. Allometry of the tendon enthesis: mechanisms of load transfer between tendon and bone. J. Biomech. Eng. 137. 111005.
Elson, E.L., Genin, G.M., 2016. Tissue constructs: platforms for basic research and drug discovery. Interface Focus 6, 20150095.
Genin, G.M., Abney, T.M., Wakatsuki, T., Elson, E.L., 2011. Cell-cell interactions and the mechanics of cells and tissues observed in bioartificial tissue constructs. In: Mechanobiology of Cell-Cell and Cell-Matrix Interactions. Springer, pp. 75–103.
Genin, G.M., Birman, V., 2009. Micromechanics and structural response of functionally graded, particulate-matrix, fiber-reinforced composites. Int. J. Solids Struct. 46, 2136–2150.

Genin, G.M., Elson, E.L., 2014. Mechanics of cell-seeded ECM scaffolds. Cell Matrix Mech., 173
Genin, G.M., Kent, A., Birman, V., Wopenka, B., Pasteris, J.D., Marquez, P.J., Thomopoulos, S., 2009. Functional grading of mineral and collagen in the attachment of tendon to bone. Biophys. J. 97, 976–985.
Grashoff, C., Aszódi, A., Sakai, T., Hunziker, E.B., Fässler, R., 2003. Integrin-linked kinase regulates chondrocyte shape and proliferation. EMBO Rep. 4, 432–438.
Guilak, F., Erickson, G.R., Ting-Beall, H.P., 2002. The effects of osmotic stress on the viscoelastic and physical properties of articular chondrocytes. Biophys. J. 82, 720–727.
Haug, H., 1986. History of neuromorphometry. J. Neurosci. Meth. 18, 1–17.
Heath, J.P., Peachey, L.D., 1989. Morphology of fibroblasts in collagen gels: a study using 400 kev electron microscopy and computer graphics. Cell Motility Cytoskeleton 14, 382–392.
Lee, K.H., Chung, K., Chung, J.M., Coggeshall, R.E., 1986. Correlation of cell body size, axon size, and signal conduction velocity for individually labelled dorsal root ganglion cells in the cat. J. Comparative Neurol. 243, 335–346.
Lee, S.L., Nekouzadeh, A., Butler, B., Pryse, K.M., McConnaughey, W.B., Nathan, A.C., Legant, W.R., Schaefer, P.M., Pless, R.B., Elson, E.L., et al., 2012. Physically-induced cytoskeleton remodeling of cells in three-dimensional culture. PloS One 7. e45512.
Liu, Y., Schwartz, A.G., Birman, V., Thomopoulos, S., Genin, G.M., 2014. Stress amplification during development of the tendon-to-bone attachment. Biomech. Model. Mechanobiol. 13, 973–983.
Marquez, J.P., Elson, E.L., Genin, G.M., 2010. Whole cell mechanics of contractile fibroblasts: relations between effective cellular and extracellular matrix moduli. Philos. Trans. Roy. Soc. London A: Math. Phys. Eng. Sci. 368, 635–654.
Marquez, J.P., Genin, G.M., Pryse, K.M., Elson, E.L., 2006. Cellular and matrix contributions to tissue construct stiffness increase with cellular concentration. Ann. Biomed. Eng. 34, 1475–1482.
Marquez, J.P., Genin, G.M., Zahalak, G.I., Elson, E.L., 2005a. The relationship between cell and tissue strain in three-dimensional bio-artificial tissues. Biophys. J. 88, 778–789.
Marquez, J.P., Genin, G.M., Zahalak, G.I., Elson, E.L., 2005b. Thin bio-artificial tissues in plane stress: the relationship between cell and tissue strain, and an improved constitutive model. Biophys. J. 88, 765–777.
Mayhew, T., Cruz, L., 1973. Stereological correction procedures for estimating true volume proportions from biased samples. J. Microsc. 99, 287–299.
Mayhew, T., Cruz Orive, L.M., 1974. Caveat on the use of the delesse principle of areal analysis for estimating component volume densities. J. Microsc. 102, 195–207.
Milton, G.W., 2002. The theory of composites. The Theory of Composites, by Graeme W. Milton, p. 748. ISBN 0521781256. Cambridge University Press, Cambridge, UK, May 2002, 748.
Mouton, P.R., 2002. Principles and Practices of Unbiased Stereology: An Introduction for Bioscientists. JHU Press.
Mouton, P.R., 2014. Quantitative anatomy using design-based stereology. Approx. Anal. Meth. Solving Ordinary Differ. Equ., 217
Nekouzadeh, A., Pryse, K.M., Elson, E.L., Genin, G.M., 2008. Stretch-activated force shedding, force recovery, and cytoskeletal remodeling in contractile fibroblasts. J. Biomech. 41, 2964–2971.
Plumley, W.C., Kostrna, M., Goodman, S.L., 2019. Cryo-planing biological specimens for scanning electron microscopy. Microsc. Today 27, 20–25.
Saadat, F., Birman, V., Thomopoulos, S., Genin, G.M., 2015. Effective elastic properties of a composite containing multiple types of anisotropic ellipsoidal inclusions, with application to the attachment of tendon to bone. J. Mech. Phys. Solids 82, 367–377.
Saadat, F., Deymier, A.C., Birman, V., Thomopoulos, S., Genin, G.M., 2016. The concentration of stress at the rotator cuff tendon-to-bone attachment site is conserved across species. J. Mech. Behav. Biomed. Mater. 62, 24–32.
Soares, J.S., Sacks, M.S., 2016. A triphasic constrained mixture model of engineered tissue formation under in vitro dynamic mechanical conditioning. Biomech. Model. Mechanobiol. 15, 293–316.
Spencer, T.M., Blumenstein, R.F., Pryse, K.M., Lee, S.L., Glaubke, D.A., Carlson, B.E., Elson, E.L., Genin, G.M., 2016. Fibroblasts slow conduction velocity in a reconstituted tissue model of fibrotic cardiomyopathy. ACS Biomater. Sci. Eng. 3, 3022–3028.
Svoronos, A.A., Tejavibulya, N., Schell, J.Y., Shenoy, V.B., Morgan, J.R., 2013. Micro-mold design controls the 3d morphological evolution of self-assembling multicellular microtissues. Tissue Eng. Part A 20, 1134–1144.
Thomopoulos, S., Birman, V., Genin, G.M., 2012. Structural Interfaces and Attachments in Biology. Springer Science & Business Media.
Thomopoulos, S., Das, R., Birman, V., Smith, L., Ku, K., Elson, E.L., Pryse, K.M., Marquez, J.P., Genin, G.M., 2011. Fibrocartilage tissue engineering: the role of the stress environment on cell morphology and matrix expression. Tissue Eng. Part A 17, 1039–1053.
Thomopoulos, S., Genin, G.M., Galatz, L.M., 2010. The development and morphogenesis of the tendon-to-bone insertion what development can teach us about healing. J. Musculoskeletal Neuronal Interact. 10, 35.
Thomopoulos, S., Marquez, J.P., Weinberger, B., Birman, V., Genin, G.M., 2006. Collagen fiber orientation at the tendon to bone insertion and its influence on stress concentrations. J. Biomech. 39, 1842–1851.
Wagenseil, J.E., Wakatsuki, T., Okamoto, R.J., Zahalak, G.I., Elson, E.L., 2003. One-dimensional viscoelastic behavior of fibroblast populated collagen matrices. J. Biomech. Eng. 125, 719–725.
Wang, H., Abhilash, A., Chen, C.S., Wells, R.G., Shenoy, V.B., 2014. Long-range force transmission in fibrous matrices enabled by tension-driven alignment of fibers. Biophys. J. 107, 2592–2603.
Weibel, E.R., Kistler, G.S., Scherle, W.F., 1966. Practical stereological methods for morphometric cytology. J. Cell Biol. 30, 23–38.
Wong, M., Wuethrich, P., Eggli, P., Hunziker, E., 1996. Zone-specific cell biosynthetic activity in mature bovine articular cartilage: a new method using confocal microscopic stereology and quantitative autoradiography. J. Orthopaedic Res. 14, 424–432.
Zemel, A., Safran, S., 2007. Active self-polarization of contractile cells in asymmetrically shaped domains. Phys. Rev. E 76. 021905.